Theoretical Calculation of Polymer Deposition Thickness on a Cylindrical Substrate

Mark B. Shiflett
Dept. of Chemical Engineering, University of Delaware, Newark, DE 19716
and
DuPont Central Research and Development Experimental Station, Wilmington, DE 19880

Henry C. Foley
Dept. of Chemical Engineering, Pennsylvania State University, University Park, PA 16802

Akimichi Yokozeki
DuPont Fluoroproducts Laboratory, Chestnut Run Plaza, Wilmington, DE 19880

A theoretical model developed predicts the thickness of a polymer film, coated on a rotating and translating cylindrical support. A model for the deposition process can be used to determine optimal operating conditions. It was validated experimentally and shows that the film-thickness morphology is quite sensitive to certain operating parameters. For example, particular sets of operating parameter values can produce highly nonuniform film thicknesses. Selected examples of the model calculations are discussed, as well as their implications.

Introduction

Coating polymer films onto various substrates is common practice in many industrial applications. Usually these applications require the precise and controlled thickness of the films (Persoons and Van Brussel, 1993; Vivekanandhan et al., 1994). Furthermore, controlling thickness is an important factor in avoiding cracking during curing processes since it is well-known that there exists a critical cracking thickness, below which the film has mechanical properties that are more plastic-like than in the bulk (Hutchinson and Suo, 1991).

Recently, we have prepared continuous nanoporous carbon (NPC) membranes (Chen and Yang, 1994; Rao and Sircar, 1993, 1996; Kasakabe et al., Singh-Ghosal and Koros, 2000) as thin films supported on porous stainless-steel tubes (Acharya et al., 1997; Acharya and Foley, 1999, 2000; Shiflett and Foley, 1999). The porous stainless tube was coated with a solution of poly(furfuryl) alcohol using an ultrasonic spray apparatus; see Figure 1 (Shiflett and Foley, 2001). To produce the carbon, the polymer was pyrolyzed on the support in an inert atmosphere. These NPC membranes prepared in this way showed an unprecedented molecular selectivity in permeation and transport. However, one difficulty encountered in the manufacturing of these NPC membranes was micro-crack formation during pyrolysis due to nonuniform film thickness. It was estimated that the onset of catastrophic film cracking occurs in the vicinity of a critical film thickness of 20 μm (Shiflett et al., 2000). This problem reduces the reproducibility of the membrane synthesis process. At the same time, it was found that the film thickness cannot be too thin or else the high selectivity produced by molecular transport is lost. Thus, the polymer deposition process must be carefully controlled in order to produce membranes with the desired thickness and uniformity, reproducibly.

Several operating parameters are related to the control of the film thickness and uniformity. Rotational and translational speeds of the cylindrical substrate, the number of repeated coatings, the geometrical relationship between the ultrasonic spray-nozzle (Hueter and Bolt, 1960; Frederick, 1965; Ensminger, 1973; Suslick, 1988) and the substrate, the flux of the polymer solution to the substrate, and the degree of angular spread of the spray beam each contribute to uniformity and thickness. Hence, a theoretical model that relates each of these parameters to a prediction of film thickness and uniformity is highly desired. Surprisingly little has been done previously toward this goal. There are at least two theoretical models in the literature that describe spray coating (Figueroa and Diaz, 1992; Hansbo and Nylen, 1999) and other work on

Correspondence concerning this article should be addressed to A. Yokozeki.

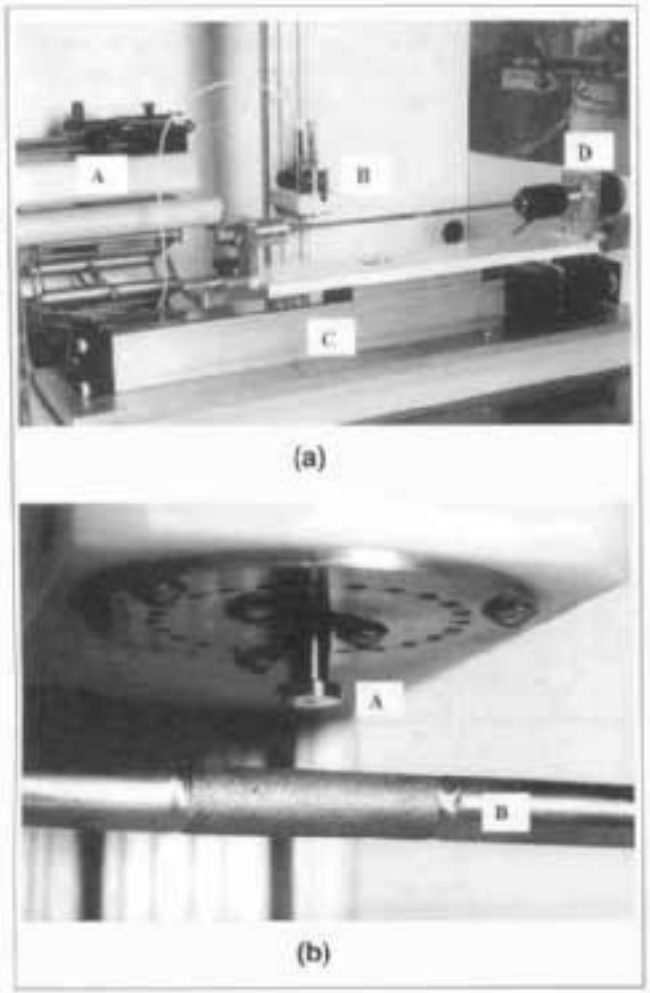

Figure 1. (a) Overview picture of polymer coating apparatus, (b) enlarged view of ultrasonic spray nozzle system.

In (a), A: syringe pump to regulate the flow of polymer solution; B: ultrasonic spray nozzle; C: unit for translational motion of cylinder; D: electric motor for cylinder rotation. An electronic controller is not shown here. In (b), A: ultrasonically vibrating nozzle head; B: cylindrical support to be coated.

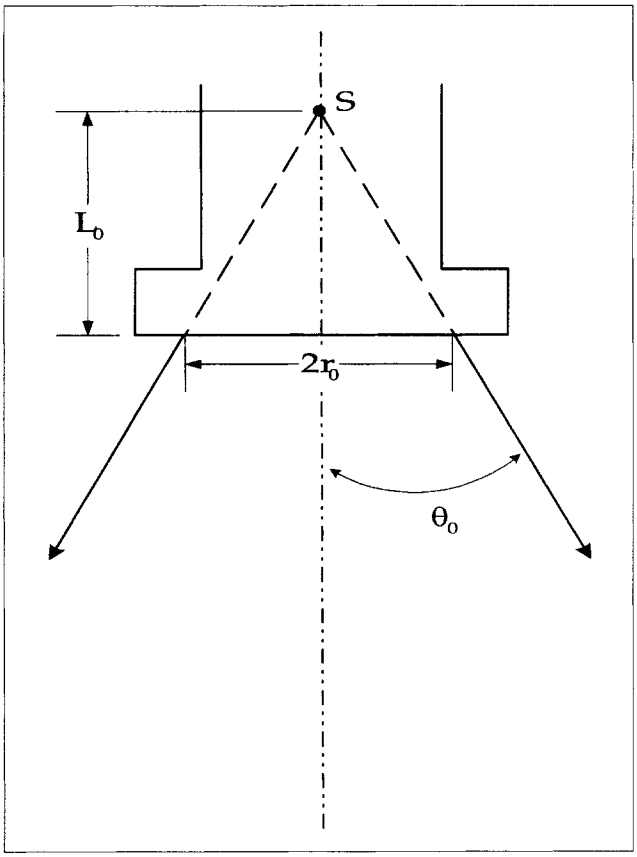

Figure 2. Geometrical definition of spray nozzle.

S: hypothetical point source of spray beam; r_0: effective radius of spray beam at nozzle face; and θ_0: angle of spray beam spread, $\tan \theta_0 = r_0/L_0$.

thermal spray coating (Fasching et al., 1993; Goedjen et al., 1995; Leigh and Berndt, 1997; Montillet et al., 1998; Nylen et al., 1996), but no theoretical model describes the problem of coating a translating and rotating tube. Therefore, we have developed a general model for this procedure.

Experimental Procedure

Since the spray beam's characteristics are important for the development of the coating model, we conducted a series of experiments to determine the quantitative relation between the volume flow rate ($\dot{V}$) and the beam's angular spread (θ_0) and effective radius (r_0) (see Figure 2). Experiments were performed by spraying flat sheets of paper with polymer solution at various distances (L_1) from the nozzle head. By measuring the resultant coating's width with varying L_1 and $\dot{V}$, the relationships between θ_0, r_0, and $\dot{V}$ were obtained. For example, in the case of a solution of 30 mass percent polymer in acetone, we found the following correlation: $r_0 = 0.0458 + 0.5191\sqrt{\dot{V}}$, and $\theta_0 = -18.14 + 326.3\dot{V} - 499.0\dot{V}^2$: r_0 in cm, θ_0 in degrees, and $\dot{V}$ in $\text{cm}^3 \cdot \text{min}^{-1}$ (for $0.1 \le \dot{V} \le 0.3$ $\text{cm}^3 \cdot \text{min}^{-1}$). For solutions with different concentrations, the numerical coefficients of these equations differed, and the higher the polymer concentration, the smaller was the angular spread (θ_0) of the beam.

Liquid densities (ρ_0) of the polymer/acetone solution were measured, since this information was also needed in the coating model. An empirical density correlation was derived: $\rho_0 = 0.7827 + 0.3175w + 0.1112w^2$ at 25°C with ρ_0 in $\text{g} \cdot \text{cm}^{-3}$, and w the mass fraction of the polymer in acetone (for $0 \le w \le 1$).

To validate the coating model calculations, a cylindrical support was wrapped with a sheet of paper and sprayed with poly(furfuryl) alcohol using the ultrasonic spray system. The support diameter, $2d = 2.54$ cm, and the paper sample dimensions were 3.14 cm × 10.16 cm. The distance from the nozzle face to the cylinder surface, $L_1 = 2.22$ cm, mass fraction of polymer concentration, $w = 0.3$, polymer-solution flow rate, $\dot{V} = 0.2$ $\text{cm}^3 \cdot \text{min}^{-1}$, rotational frequency, $f_R = 1.0$ s^{-1}, coverage distance measured in the axial direction, $L' = 7.62$ cm, and number of coating passes, $N = 16$, remained constant. Two different translational velocities, v_z, were tested

0.7645 cm·s^{-1} and 0.6850 cm·s^{-1}. The ultrasonic nozzle was powered by a generator operating at 2.0 J·s^{-1}. The samples were allowed to air dry for 24 h, and were imaged using a UMAX PowerLook 2000 scanner operating in reflection mode. The images were scanned in color with a resolution of 100 dots per inch. Reference samples with known masses of poly(furfuryl) alcohol polymer were also sprayed to calibrate color intensity with polymer thickness.

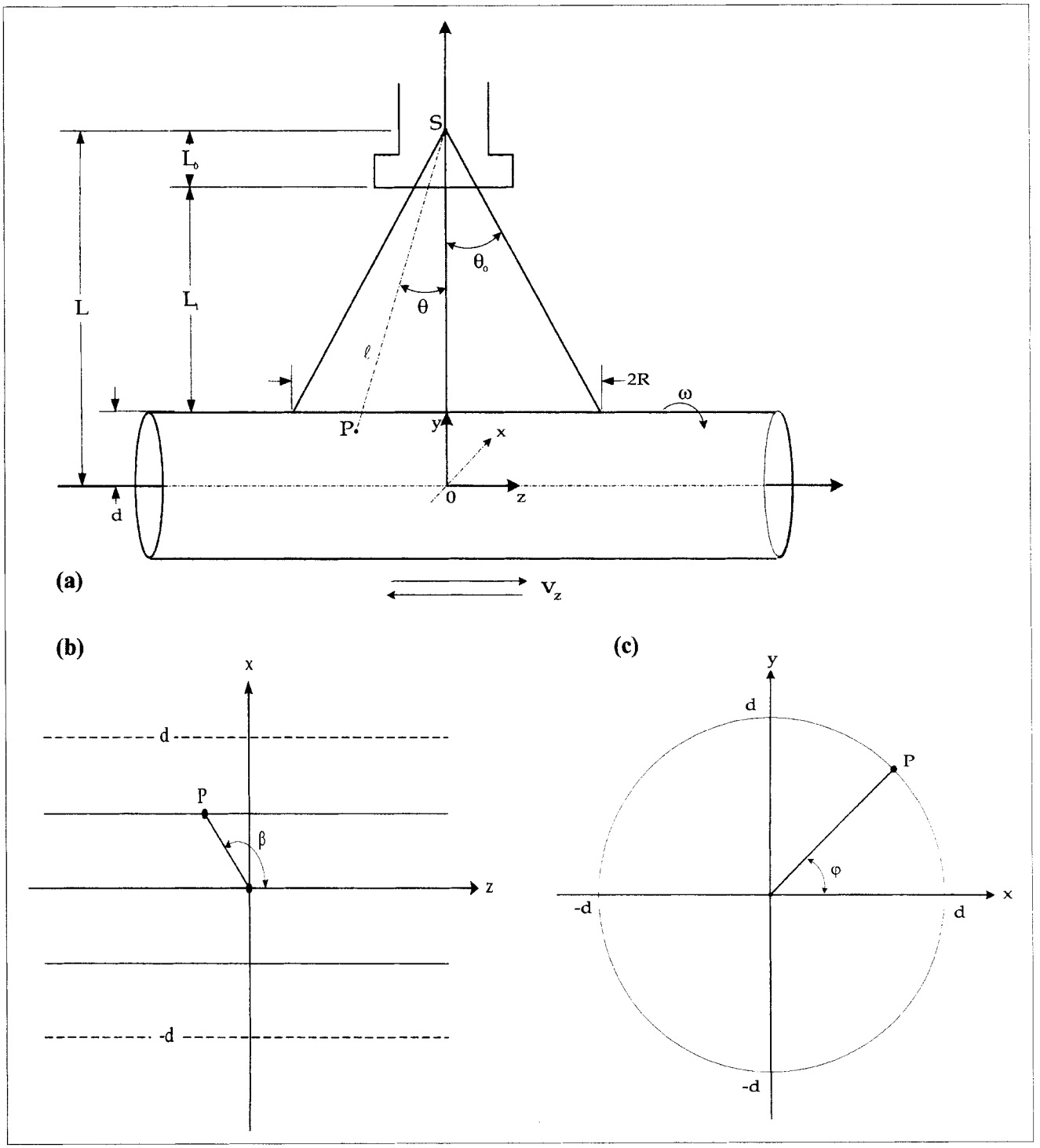

Figure 3. Definition of coordinates and symbols for spray nozzle and cylindrical support.

(a) View of spray coating on cylinder surface. S: hypothetical point source of spray beam; P: arbitrary point on the cylinder (radius d) surface; ω: angular frequency of rotating cylinder; v_z: translational velocity of cylinder in forward and backward direction; and θ_0: angle of spray beam spread, $\tan\theta_0 = R/L_1$. (b) Cross section of x,z-plane containing the point, P, and definition of angle, β. (c) Cross section of x,y-plane containing the point, P, and definition of phase angle φ.

Model Development

First we consider the case of a stationary cylindrical surface. Figures 2 and 3 illustrate the geometrical relationship between the spray nozzle and a coating cylinder. Then, an arbitrary point, $P(x,y,z)$, on the cylinder surface can be located as follows

$$x = l \sin\theta \sin\beta = d \cos\varphi \tag{1}$$

$$y = L - l \cos\theta = d \sin\varphi \tag{2}$$

$$z = l \sin\theta \cos\beta, \tag{3}$$

where L is given by

$$L = L_0 + L_1 + d = r_0/\tan\theta_0 + L_1 + d, \tag{4}$$

and the distance, l, is measured from the hypothetical point source of spray beam S to point P on surface in Figure 3. It is convenient to express l in terms of the variables, z and φ, for later use. This can be easily done by eliminating the θ and β variables using Eqs. 1, 2, and 3.

$$l^2 = z^2 + d^2 + L^2 - 2Ld \sin\varphi. \tag{5}$$

Now, consider a small area of surface, dS around the point P, in contact with a volume V containing N spray particles (see Figure 4). Our problem is to calculate the frequency of particles hitting the surface, that is, the number of particles that strike the surface, dS, in unit time. Imagine an average particle velocity of magnitude $\bar{c}$, the direction of which lies within a solid angle, dS/l^2, at an angle θ. In a time interval dt, particles with velocity $\bar{c}$ will hit the surface provided they are within a distance $\bar{c}dt \cos\gamma$ from the surface. If there are N/V particles per unit volume, the number of such particles striking unit area in the θ direction is

$$dN = (N/V)\bar{c} \cos\gamma \, dt. \tag{6}$$

Next, we assume that all striking particles having an average mass $\bar{m}$ will be deposited on the surface dS during the time dt and form a small coated volume, $dS \cdot dh_x$, with a thickness of dh_x and a polymer solution density of ρ_0. Then, it holds that $dN\bar{m}dS = dSdh_x\rho_0$. However, the solvent of the polymer solution will be evaporated, leaving the polymer material on the surface with a thickness of dh and a polymer density of ρ. So, we assume $dh_x\rho_0 = dh\rho + (dh_x - dh)\rho_s$ (a simple mass conservation), where ρ_s is the solvent liquid density. Then, the preceding equation can be written in terms of the dry polymer thickness, dh: $dN\bar{m}\,dS = dS\,dh\rho_0(\rho - \rho_s)/(\rho_0 - \rho_s)$. By inserting this relation into Eq. 6 and rearranging the equation the following differential equation is obtained for the coated thickness of polymers

$$\frac{dh}{dt} = \frac{\rho_0 - \rho_s}{\rho_0(\rho - \rho_s)} \frac{N\bar{m}\bar{c}}{V} \cos\gamma. \tag{7}$$

Here the term $N\bar{m}\bar{c}/V$ is a mass flux of spray particles around the point P, within a solid angle, dS/l^2, at an angle θ.

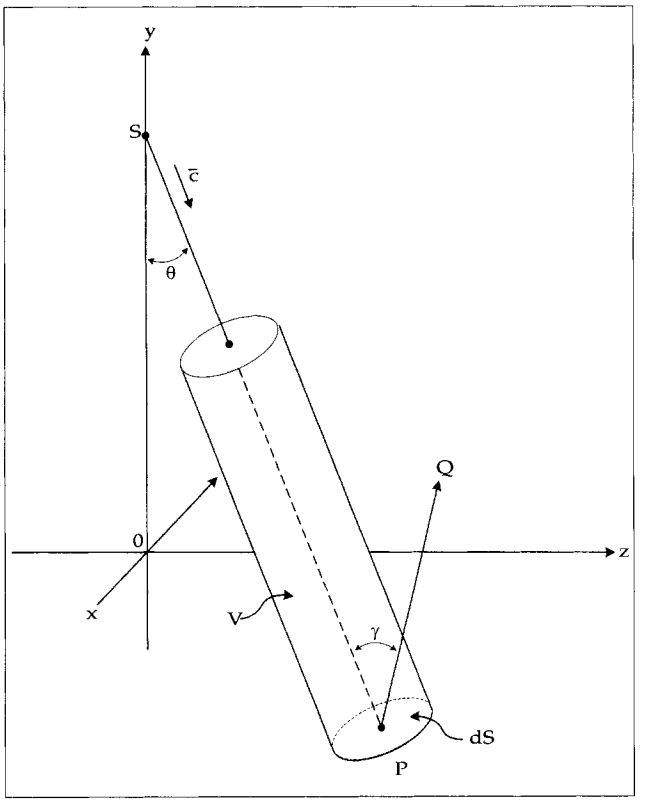

Figure 4. Geometry of a spray beam striking the surface point *P* of cylinder.

$\bar{c}$: average speed of spray particles; S: hypothetical point source of spray beam; $\overline{PQ}$: unit vector normal to a small surface dS; V: small volume containing striking spray particles; $\overline{SP}$: spray-beam vector at angle θ; and γ: angle between $\overline{PQ}$ and $\overline{SP}$ vectors.

On the other hand, the total mass flux at the hypothetical point-source is given by $(\dot{V}\rho_0/\pi r_0^2)$, where $\dot{V}$ is the volume flow rate of the polymer solution with density ρ_0, and r_0 is the effective radius of the spray-nozzle head, as shown in Figure 2. Then the mass-flux term in Eq. 7 can be expressed in terms of the point-source mass flux times a solid angle reduction term, which is inversely proportional to the square of distance from the source for a given dS area. The flux reduction at point P is obtained, with respect to the same area dS at the nozzle head at the angle θ. Thus

$$\frac{N\bar{m}\bar{c}}{V} = \frac{\dot{V}\rho_0}{\pi r_0^2}\left(\frac{L_0}{l\cos\theta}\right)^2. \tag{8}$$

Using Eqs. 4 and 5 with Eq. 8, and after some algebraic manipulations, Eq. 7 becomes

$$\frac{dh}{dt} = \frac{\dot{V}(\rho_0 - \rho_s)}{\pi(\rho - \rho_s)} \frac{1}{(ad)^2 + \{a(L_1 + d) + r_0\}^2 - 2ad\{a(L_1 + d) + r_0\}\cos\varphi + (az)^2} \frac{\cos\gamma}{\cos^2\theta}, \tag{9}$$

with $a \equiv \tan\ \theta_0$.

Our next task is to discover various relationships among the free variables, γ, θ, φ, β, and z through analytical geometry, since they are not all independent of each other. First, the angle γ between the vectors SP and PQ in Figure 4 has the following relation by taking the inner product of the two unit vectors

$$\cos\gamma = \cos\theta\cos\varphi - \sin\beta\sin\theta\sin\varphi. \tag{10}$$

With the aid of Figures 3b and 3c, the relation $\tan\beta = d\cos\varphi/z$ is obtained and applying an elementary trigonometric relationship the following equations resulted

$$\sin\beta = \frac{d\cos\varphi}{\sqrt{z^2 + (d\cos\varphi)^2}}, \quad \cos\beta = \frac{z}{\sqrt{z^2 + (d\cos\varphi)^2}}. \tag{11}$$

Eliminating l from Eq. 2 and Eq. 3 and using Eq. 11 gives Eq. 12,

$$\tan\theta = \frac{a\sqrt{z^2 + (d\cos\varphi)^2}}{r_0 + a(L_1 + d - d\sin\varphi)}, \quad a \equiv \tan\theta_0. \tag{12}$$

From this equation, we obtain

$$\cos\theta = \frac{r_0 + a(L_1 + d) - ad\sin\varphi}{\sqrt{(az)^2 + (ad)^2 + (r_0 + aL_1 + ad)^2 - 2ad(r_0 + aL_1 + ad)\sin\varphi}}. \tag{13}$$

Using these angular relationships, Eqs. 10, 11, and 13, the righthand side of Eq. 9 can be expressed in terms of two variables, z and φ

$$\frac{dh}{dt} = \frac{\dot{V}(\rho_0 - \rho_s)}{\pi(\rho - \rho_s)C^2} \times \frac{\left(\sqrt{(Az)^2 + B^2 + 1 - 2B\sin\varphi} - B\sin\varphi\right)\cos\varphi}{\left(B^2 + 1 - 2B\cos\varphi + (Az)^2\right)(1 - B\sin\varphi)}, \tag{14}$$

with $A \equiv \tan\theta_0/C$, $B \equiv d\tan\theta_0/C$, and $C \equiv r_0 + (L_1 + d)\times\tan\theta_0$. It should be noted that this equation determines the differential polymer thickness at any point specified by the two variables, z and φ, with given geometrical parameters, r_0, L_1, and d.

Now we are ready to consider the effect of moving the cylinder surface. When a cylinder rotating with an angular frequency, ω, moves in the z-direction with a translational speed, v_z, the rotational phase angle φ and the z-coordinate at a time t are

$$\varphi = \omega t + \varphi_0 \tag{15}$$

$$z = -v_z t + z_0. \tag{16}$$

The point specified by (z_0, φ_0) is a proper initial starting coordinate for coating. Here, we assume that the coating cylinder moves from right to left for the first coating pass and reverses the motion for the second pass [$-v_z \rightarrow v_z$ and $z_0 \rightarrow -z_0$], while the rotational motion is always the same direction (see Figure 3). The arbitrary point $P(x, y, z)$ in Eqs. 1, 2, and 3 is now a function of t

$$x = d\cos(\omega t + \varphi_0) \tag{17}$$

$$y = d\sin(\omega t + \varphi_0) \tag{18}$$

$$z = -v_z t + z_0. \tag{16}$$

Then the coating-thickness equation, Eq. 14, becomes a function of t only, and the thickness can be obtained by integrating with t. However, it is convenient for the integration to rewrite Eq. 14 in terms of the position coordinate, z. From Eqs. 15 and 16, we have

$$\varphi = \frac{\omega(z_0 - z)}{v_z} + \varphi_0. \tag{19}$$

Using the relation $dh/dt = (dh/dz)(dz/dt) = -v_z(dh/dz)$, Eq. 14 is written in terms of z

$$\frac{dh}{dz} = \frac{-\dot{V}(\rho_0 - \rho_s)}{\pi C^2(\rho - \rho_s)v_z} \times \frac{\left(\sqrt{(Az)^2 + B^2 + 1 - 2B\sin\varphi} - B\sin\varphi\right)\cos\varphi}{\left(B^2 + 1 - 2B\cos\varphi + (Az)^2\right)(1 - B\sin\varphi)}. \tag{20}$$

The parameters A, B, and C are the same as those in Eq. 14, and φ is a function of z, given by Eq. 19. Then, the definite integral h of a "proper range" between z_i and z_j, $h[z_i, z_j]$, becomes:

$$h[z_i, z_j] = \int_{z_i}^{z_j} \frac{-\dot{V}(\rho_0 - \rho_s)}{\pi C^2(\rho - \rho_s)v_z} \times \frac{\left(\sqrt{(Az)^2 + B^2 + 1 - 2B\sin\varphi} - B\sin\varphi\right)\cos\varphi}{\left(B^2 + 1 - 2B\cos\varphi + (Az)^2\right)(1 - B\sin\varphi)}\,dz. \tag{21}$$

Unfortunately, this integral cannot be solved analytically, and must be integrated numerically. However, when the angular spread of the spray beam is zero, or nearly zero ($\theta_0 = 0$), that is, a parallel beam, it is drastically simplified, since $A \rightarrow 0$, $B \rightarrow 0$, and $C \rightarrow r_0$. The integrand becomes a simple cos φ function, and the integral is given analytically

$$h[z_i, z_j] = \frac{\dot{V}(\rho_0 - \rho_s)}{\pi r_0^2(\rho - \rho_s)\omega}\left[\sin\left(\frac{\omega(z_0 - z)}{v_z} + \varphi_0\right)\right]_{z_i}^{z_j}. \tag{22}$$

So far, we have not defined the proper ranges for integration. Determination of the integration ranges of the coating on the moving cylinder surface is a challenging task. Since the coating only occurs on a part of the moving cylinder surface under the spray "shadow"(surface coverage area of spray beam), it is sufficient for coating of any part of the cylinder to consider only the shadow area. The cylinder length is immaterial. The questions now are what the beam shadow looks like on the stationary cylinder surface, and how a point on the cylinder surface crosses the shadow area on the repetitive forward and backward motions with rotations. The proper integral range, z_i and z_j, will be obtained after studying these questions.

First, we have to look at the beam spread in the x-direction. Figure 5 clearly illustrates the situation: Case (a) for a wide spray beam and Case (b) for a narrow spray beam. The angle of θ_d or θ_x in Figures 5a and 5b limits the x-direction of the shadow, as well as the y-direction. These limiting angles are given below

$$\theta_d = \sin^{-1}(d/L) = \sin^{-1}\frac{d\tan\theta_0}{r_0 + (L_1 + d)\tan\theta_0} \tag{23}$$

and θ_x, which is more complicated, since it is a solution of the following equation

$$d\sqrt{1-\cos^2\theta_x} = (L - d\cos\theta_x)\tan\theta_0. \tag{24}$$

But it is easily solved analytically because it can be reduced to a quadratic equation in terms of $\cos\theta_x$.

Next, the shadow limit of the z-direction must be investigated. This requires the knowledge on the contour of shadow shapes. The contour of the shadow on a stationary cylinder surface is a collection of all points that have the directional

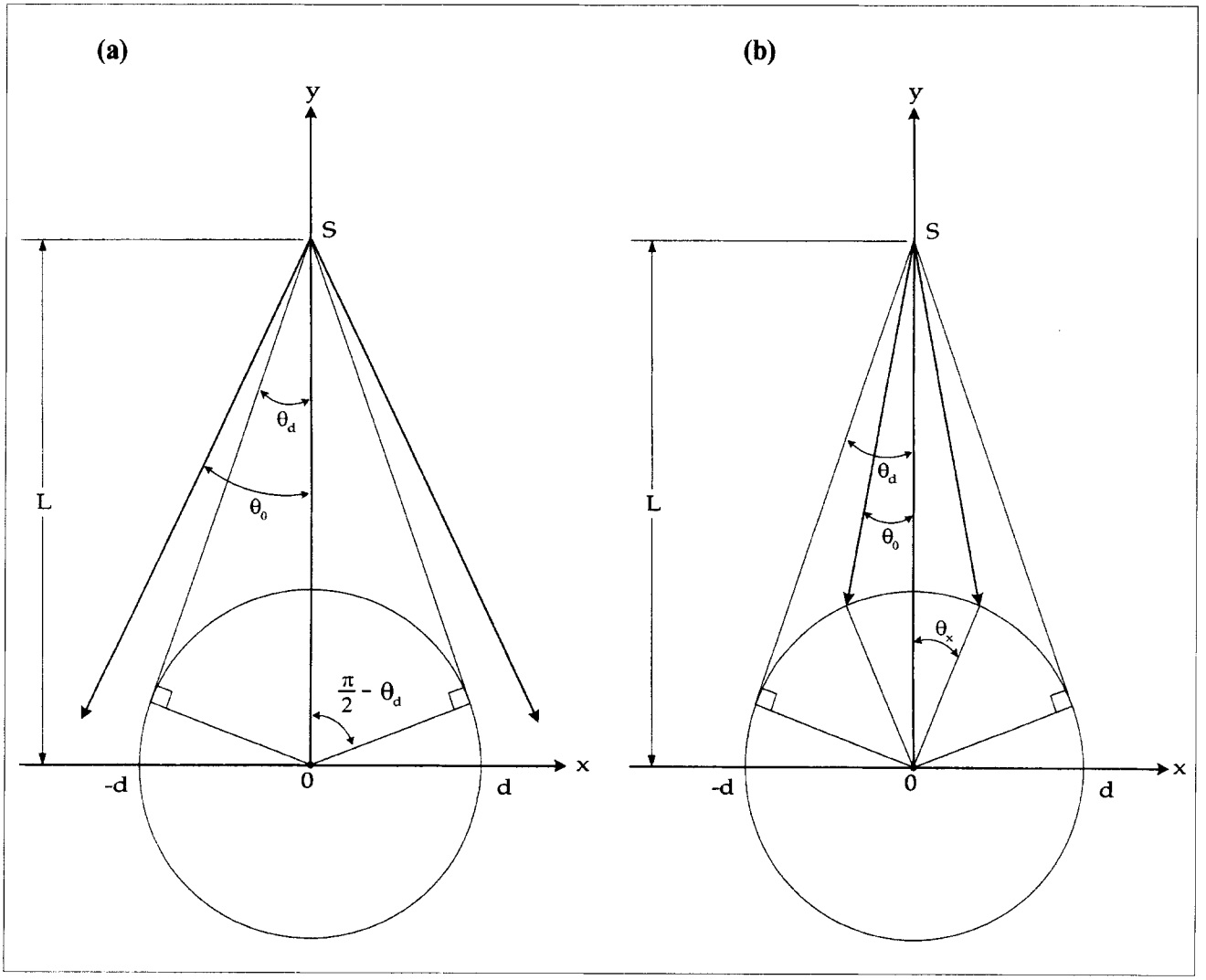

Figure 5. Limiting angles of spray beam.

Cross sections of the x, y-plane containing spray-beam angle and cylindrical support are shown. (a) Large spray-beam spread compared to diameter of cylindrical support ($\theta_0 \geq \theta_d$), and limiting angle = θ_d. (b) Large diameter of cylindrical support compared to spray-beam spread ($\theta_0 < \theta_d$), and limiting angle = θ_0.

angle of $\theta = \theta_0$ in Eqs. 1, 2, and 3, since θ_0 is the maximum angle of the spray beam. Making the sum of the squares of Eqs. 1 and 2 with $\theta = \theta_0$, and inserting Eq. 2 and sin β from Eq. 11, after some analytical manipulations we arrive at the following contour equation

$$z^2 + d^2\cos^2\varphi = \left[a(L_1 + d) + r_0 - ad\sin\varphi\right]^2, \quad a \equiv \tan\theta_0, \tag{25}$$

or, in terms of Cartesian coordinates

$$z^2 + x^2 = \left[a(L_1 + d) + r_0 - ay\right]^2, \quad a \equiv \tan\theta_0. \tag{26}$$

The allowed ranges of x, y, and φ values are limited by the limiting angles described earlier. These innocent-looking equations possess surprisingly rich features of shapes. A few examples are shown in Figure 6. They are displayed as "cut-and-opened" figures (cutting the cylinder pipe along the z-di-

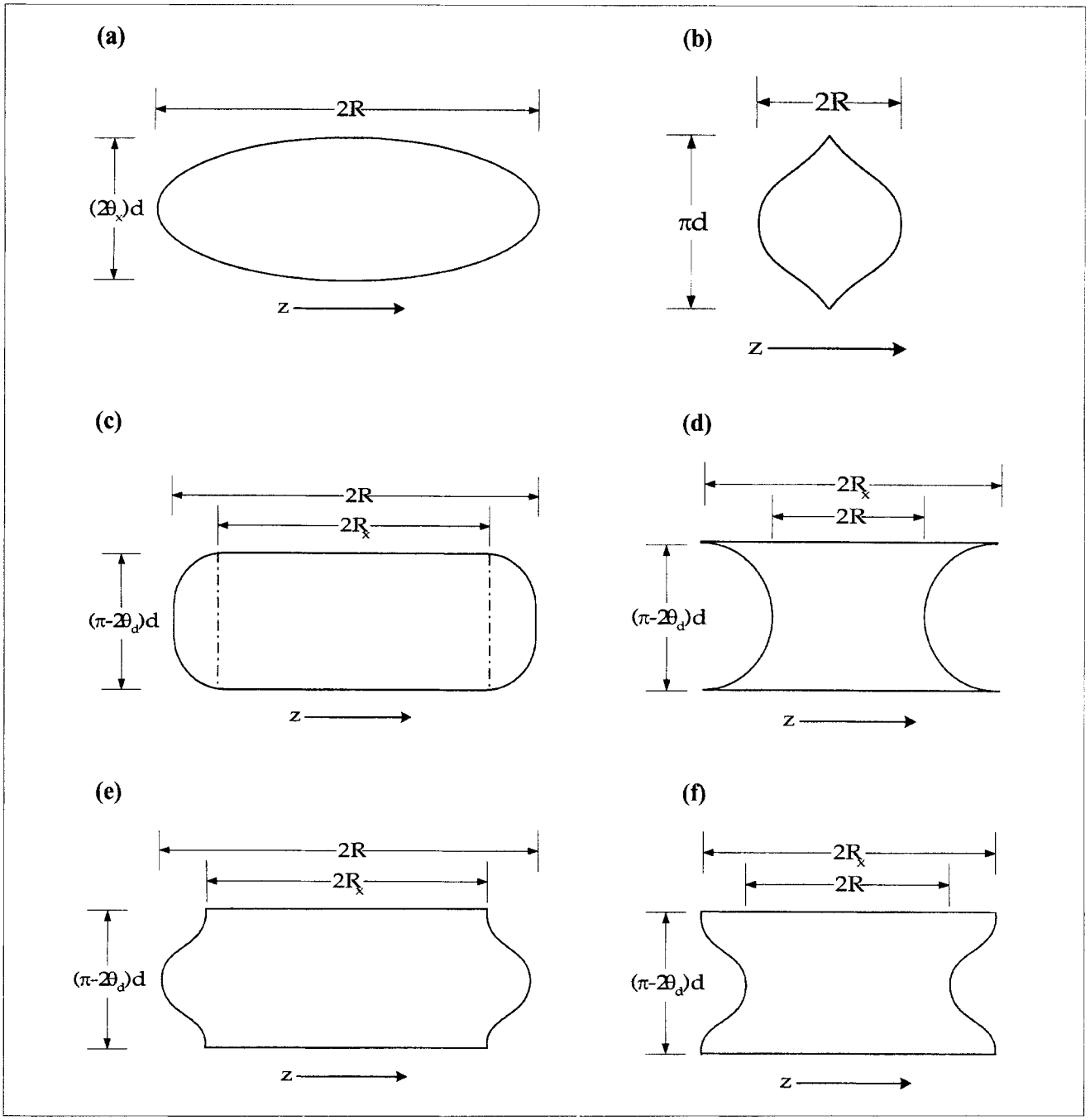

Figure 6. Examples of spray-beam coverage area on cylindrical support, shown as "cut-and-open view" along z-direction.

(a) $\theta_0 < \theta_d$ or $\theta_0 = 0$ and large d; (b) $\theta_0 = 0$ and $d = r_0$; (c) $\theta_0 = 0$ and $d \leq r_0$; (d) $\theta_0 > \theta_d$; (e) $\theta_0 = 0$ and $d \ll r_0$; (f) $\theta_0 > \theta_d$ and θ_0 larger than case (d).

rection and flattened as a sheet). The shape depends upon the combination of magnitudes of the parameters, r_0, L_1, θ_0, and d. The limits of the z-direction are shown by R and R_x: $|z| \le R$, or $|z| \le R_x$. R is simply given by $R = r_0 + L_1 \tan \theta_0$, as illustrated in Figure 3, while R_x must be solved using Eq. 25, or Eq. 26 by inserting the limit angle θ_d of Eq. 23: $x = d \cos \theta_d$, $y = d \sin \theta_d$, or $\varphi = \theta_d$.

Now, we are ready to discuss the proper integration range for Eq. 21 mentioned earlier. Any surface point on the moving cylinder will be coated by the spray beam, provided that the point is within the beam shadow. So, we have to find out when and where the point crosses the boundary of the beam shadow. This is to solve the crossing point of the shadow curve Eq. 25 or Eq. 26 and the orbit of the moving point given by Eqs. 15 and 16. In other words, the crossing point of the z-coordinate can be found by solving the roots of Eq. 25 with the rotational phase angle φ given in Eq. 19, by taking into account the limiting angle, θ_d or θ_x, and the limit $|z| \le R$ or $|z| \le R_x$. The equation to be solved is, however, highly nonlinear and multivalued, and finding proper roots, z_i, requires special attention to the numerical solutions. An example of the roots, z_i, and the shadow area is shown in Figure 7a, using the case of Figure 6d and the first coating pass. The pairs $[z_1, z_2]$, $[z_3, z_4]$, ..., $[z_{11}, z_{12}]$, shown in Figure 7a, are the proper integral ranges of Eq. 21 for the case of the starting phase angle of $\varphi_0 = \alpha_1$ and the starting z-coordinate with $z_0 = R_x$. Notice that the pair of roots, $[z_8, z_9]$ and $[z_{12}, -z_0]$, are not the proper integral range and must be excluded in this example. The second coating pass (reverse direction) is shown in Figure 7b; in this case, $\varphi_0 = \alpha_2$, and $z_0 = -R_x$. The third coating pass will be the forward direction as the first pass, but with a different $\varphi_0 = \alpha_3$ and the same $z_0 = R_x$; the fourth pass (reverse direction) as the second pass, but a different $\varphi_0 = \alpha_4$; and so forth. The phase-angle shift for each pass is derived from Eq. 19

$$\Delta\varphi_0 = \alpha_j - \alpha_i = \frac{2\omega|z_0|}{v_z}. \tag{27}$$

A view of many coating passes is given in Figure 7c, with a certain initial starting point of $\varphi_0 = \alpha_1$. In multiple coating passes, it is quite instructive to mention that when the constant phase shift of Eq. 27 has a special relation, it causes a dramatic effect on the coating pattern. That is, when the following relation holds, the coating passes will be "phase-locked" (or "frozen"); the coating pattern will be unchanged after a certain number of passes

$$\frac{\Delta\varphi_0}{2\pi} = \frac{\omega|z_0|}{\pi v_z} = \frac{2f_R|z_0|}{v_z} = \frac{n}{m}, \quad n, m = \text{integer}, \tag{28}$$

where f_R is the rotational frequency. Such examples will be shown in later sections with actual calculations.

Finally, the whole coating process for the thickness, $h_N(\varphi)$, at a radial direction φ of any z location on the cylinder after N passes may be summarized by the following symbolic equation

$$h_N(\varphi) = \sum_{k=1}^{N} \sum_{i,j}^{|z| \le z_0} h[z_i(\alpha_k), z_j(\alpha_k)], \tag{29}$$

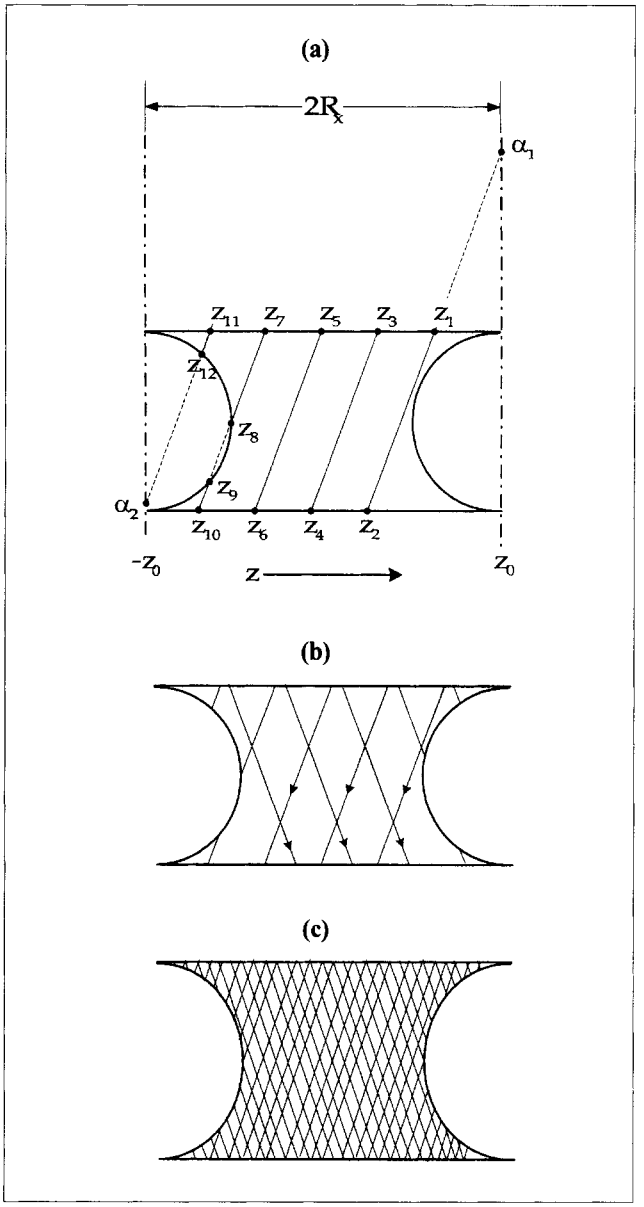

Figure 7. Example of coating passes of case (d) in Figure 6.

(a) View of one pass across cylindrical support, at starting phase angle α_1 and ending phase-angle α_2. z_i (i = 1 to 12) is a crossing point of spray-beam shadow boundary. (b) View of 2 passes across cylindrical support. (c) View of 10 passes across cylindrical support.

where $h[z_i(\alpha_k), z_j(\alpha_k)]$ is given by Eq. 21 with the proper integral range at z_i, z_j at the kth starting phase angle, $\alpha_k = \varphi + (k-1)\Delta\varphi_0$, and $z_0 = R$, or R_x.

Model Calculations

Computer programming

A computer code to calculate the thickness of polymer coating has been developed based on the theoretical model described in the previous section. The programming was fairly complicated and tedious. This was due to various factors, including root solving of multivalued nonlinear equations, tak-

ing the correct sign of trigonometric functions, sorting out and bookkeeping the proper roots, paying attention to the accuracy and convergence of numerical integration, and graphical representation of the results. An outline of the code is illustrated by a flow chart in Figure 8.

The basic inputs of the operating parameters are L_1 (the distance from the nozzle face to the cylinder surface), d (radius of the cylinder), $\dot{V}$ (polymer solution flow rate), v_z (translational speed), f_R (rotational frequency: angular frequency $\omega = 2\pi f_R$), and w (mass fraction of polymer in solvent). The densities, ρ (polymer density), ρ_0 (polymer solution density), and ρ_s (solvent density), as well as θ_0 and r_0, are calculated from the empirical correlation mentioned previously in the experimental section.

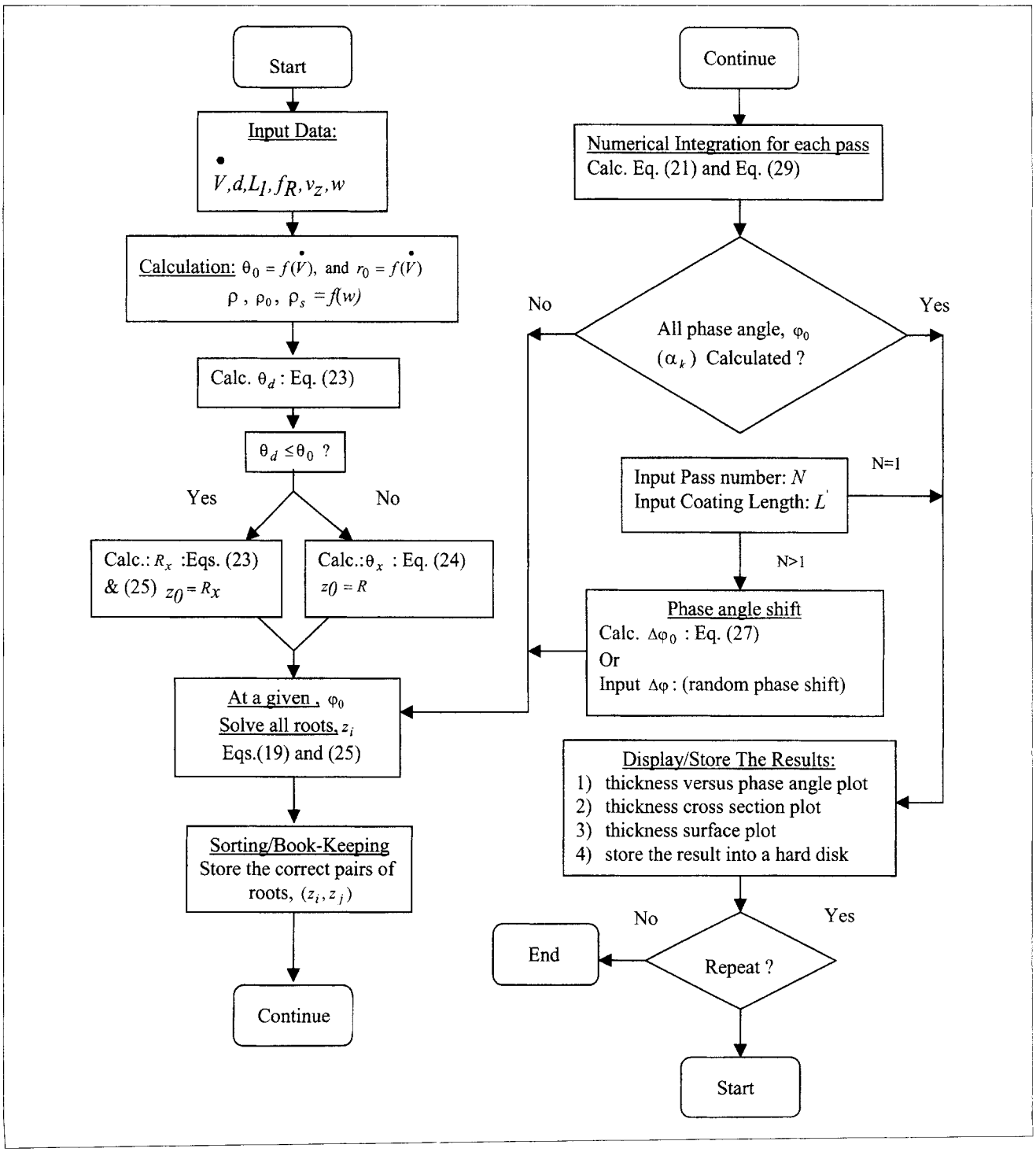

Figure 8. Flow chart of computer code.

The spatial resolution in numerical calculations is controlled by a specified angular resolution $\Delta\varphi$ in the phase angle φ. The resolution along the cylinder z-direction is given by $\Delta z = v_z \Delta\varphi/\omega$ from Eq. 19, and that in the circumference of the cylinder cross section is given by $d\Delta\varphi$. Typically, a sufficient accuracy is obtained by setting $\Delta\varphi$ of 5° ($\approx 0.028\pi$ rad).

For multiple coatings, the number of coating passes, N, and the choice of the phase-angle shift (use the constant shift of Eq. 27 or random shift) can be specified as the input data. The constant phase-angle shift assumes that the dwelling time at the reversing direction of the translational motion is zero or negligible. The random phase shift means that the dwelling time is sufficiently large and random; so, the starting phase angle at each reversing time is randomly distributed within a specified angle (input data). For certain applications, this option may be useful for examining such uncontrolled effects.

After all necessary calculations have been made, the numerical results are stored in a hard disk and graphically displayed on a computer video screen. Three display options are provided for viewing the coating thickness and uniformity: (1) axial view at a specified phase-angle position; (2) cross-section view; (3) 3-dimensional (3-D) surface plot.

In addition to the preceding program, a supplemental computer code has been created in order to gain further insights of the coating process. This program provides graphical presentations of the beam-spray area and coating pass process such as those in Figures 6 and 7, and the numerical information of the phase-lock condition given by Eq. 28.

Examples of theoretical calculations

Selected examples from a series of computer simulations were chosen to show the sensitivity in the coating-thickness variability with respect to operating variables. The basic inputs of the operating parameters are L_1, d, $\dot{V}$, w, v_z, and f_R, as mentioned previously in the computer programming section. Proper values were chosen in order to simulate a realis-

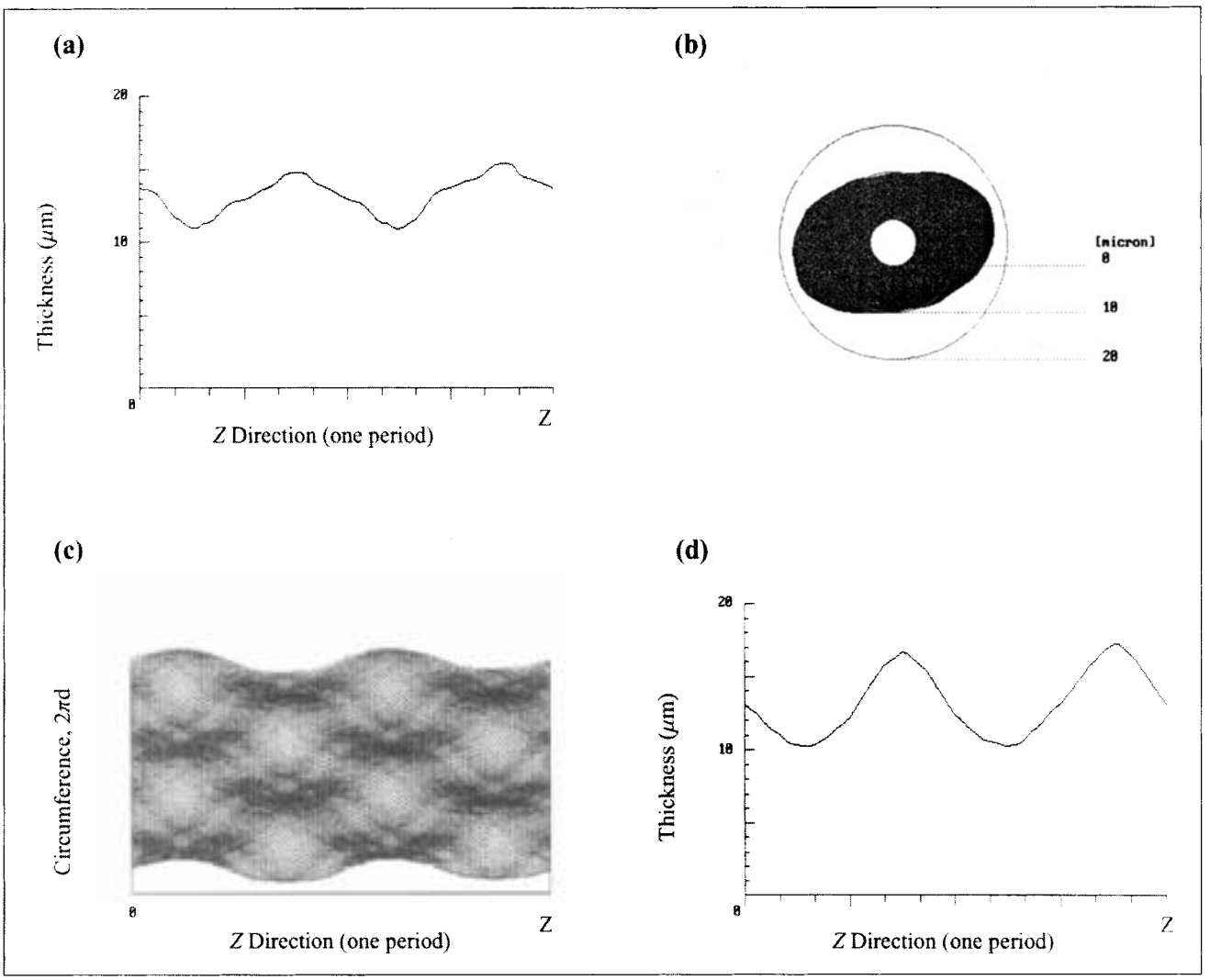

Figure 9. Results of computer simulation with $f_R = 1.0\ s^{-1}$, $\dot{V} = 0.2\ cm^3 \cdot min^{-1}$; $N = 10$; $v_z = 0.965\ cm \cdot s^{-1}$; $2R_x = 1.690$ cm.

(a) Axial view at $\varphi = 45°$; (b) cross-section view at $z = R_x/3$; (c) 3-D surface plot; (d) axial view at $\varphi = 45°$, with random phase shift 10°.

tic condition used in the previous experiments (Shiflett and Foley, 2000). The distance from the nozzle face to the cylinder surface, $L_1 = 0.9525$ cm, diameter of the tubular support, $2d = 0.6350$ cm, mass fraction of polymer concentration, $w = 0.3$, polymer solution flow rate, $\dot{V} = 0.2$ cm^3·min^{-1}, rotational frequency, $f_R = 1.0$ s^{-1}, and number of coating passes, $N = 10$, were set as constants in these examples. Only the translational speed was varied from $v_z = 0.846$ cm·s^{-1} to 0.965 cm·s^{-1}. With the present $\dot{V}$ and w, the spray-beam half-angle is $\theta_0 = 27.2°$, and the effective spray-nozzle diameter is $2r_0 = 0.556$ cm.

The angular resolution $\Delta\varphi$ of 5° was used; in terms of the spatial surface resolutions, those in the cylinder z-direction and in the direction perpendicular to z were about 13 μm and 280 μm, respectively, with the preceding input data. The computer code ran on a PC operating system, and with the present resolution ($\Delta\varphi$ of 5°), these calculations took about 10 to 15 s on a 200-MHz processor.

The first example simulates a coating sprayed at $v_z = 0.965$ cm·s^{-1}. Figure 9a provides an axial view at $\varphi = 45°$ which clearly shows the nonuniformity in the coating thickness along the z-direction. The coating has an average thickness of 12.8 μm, with a sinusoidal variability of about ± 2.0 μm at a phase angle, $\varphi = 45°$. Another way to view this is by the cross section shown in Figure 9b. One can easily see that the coating thickness varies from 10 μm to 17 μm. Figure 9c provides a 3-D surface plot of the cylinder surface cut and opened along the z-direction and flattened as a sheet. The "hills and valleys" in the coating can clearly be seen. This high degree of variability in the coating thickness can lead to crack formation in the carbon films during pyrolysis, rendering the membranes useless for gas separation. The effect of including a random phase-angle shift, $\Delta\varphi = 10°$ is shown in Figure 9d. The average thickness remains the same. However, the variability in coating has increased from ± 2.0 μm to ± 3.0 μm.

The second example was run at the same conditions, except the translational speed was lowered, $v_z = 0.889$ cm·s^{-1}. This provided a significant improvement in the coating uniformity. Figure 10a provides an axial view, $\varphi = 45°$, which shows an average thickness of 14.5 ± 0.3 μm, almost an order

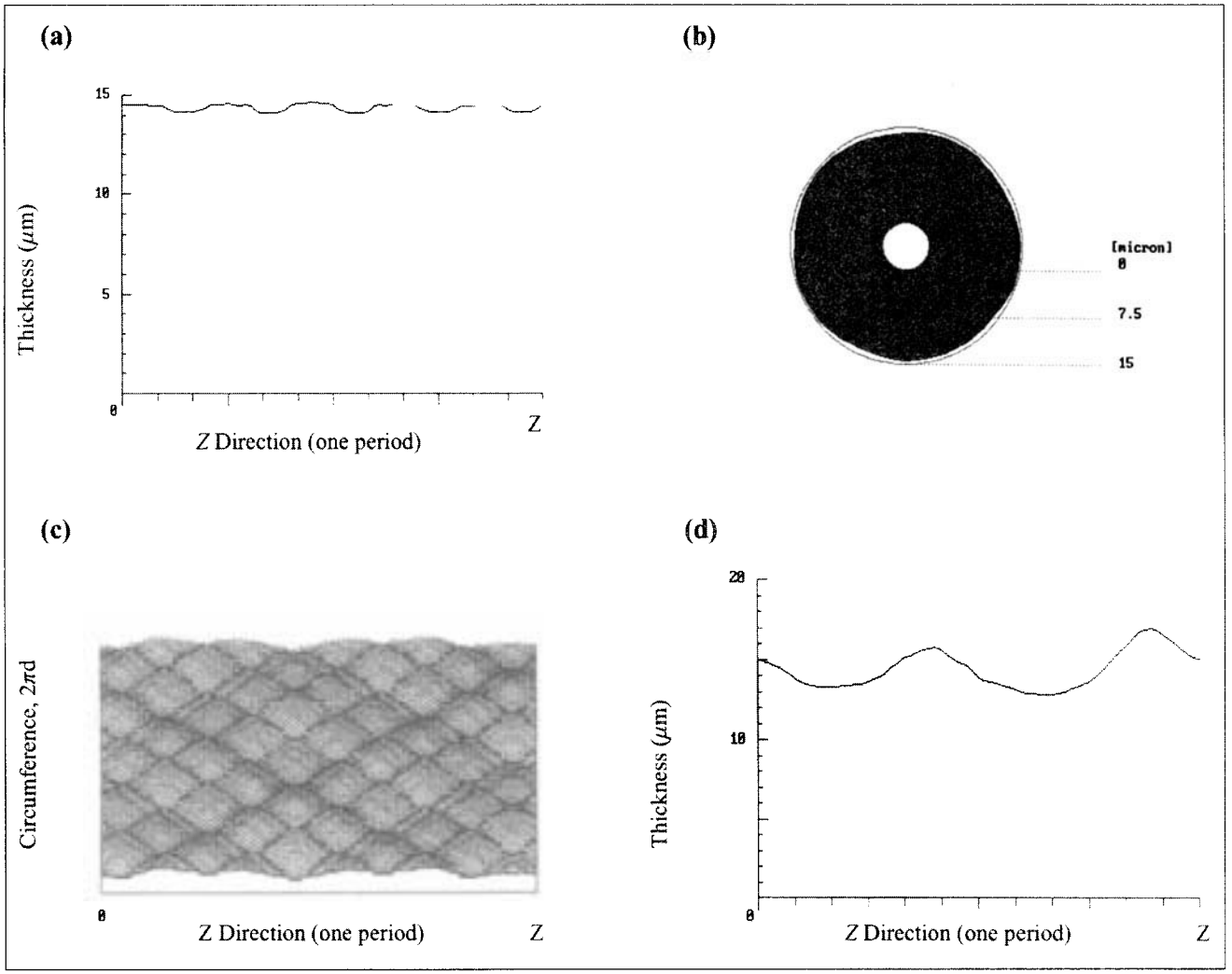

Figure 10. Results of computer simulation with the same parameters as those in Figure 9, except $v_z = 0.889$ cm·s^{-1}; $2R_x = 1.690$ cm.

(a) Axial view at $\varphi = 45°$; (b) cross-section view at $z = R_x/3$; (c) 3-D surface plot; (d) axial view at $\varphi = 45°$, with random phase shift 10°.

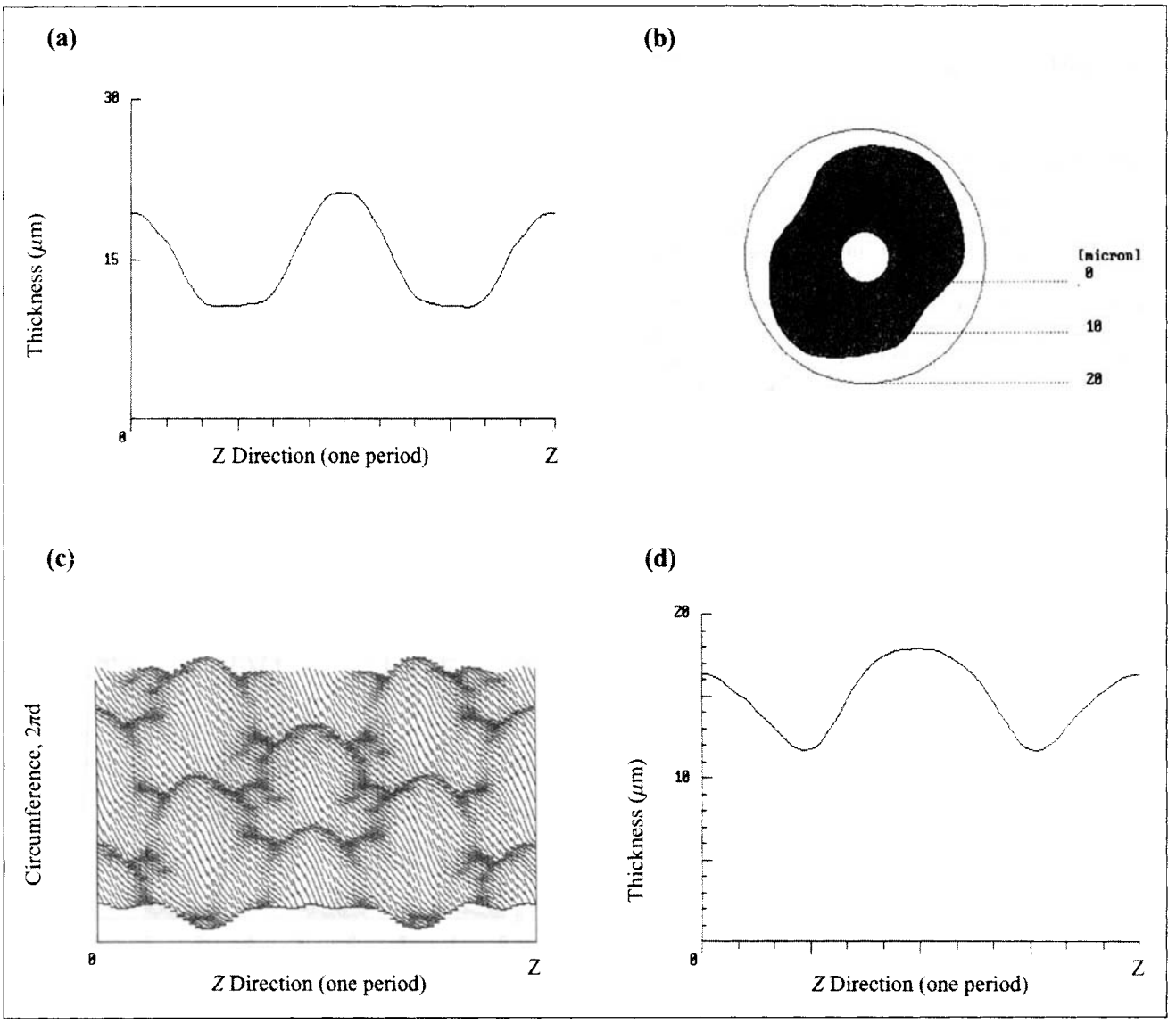

Figure 11. Results of computer simulation with the same parameters as those in Figure 9, except $v_z = 0.846$ cm·sec^{-1}; $2R_x = 1.690$ cm.

(a) Axial view at $\varphi = 45°$; (b) cross-section view at $z = R_x/3$; (c) 3-D surface plot; (d) axial view at $\varphi = 45°$, with random phase shift 10°.

of magnitude improvement in coating thickness variability compared with the previous example. The cross-section view, Figure 10b, and the 3-D surface plot, Figure 10c, also confirm the improved uniformity in the coating thickness. The significance of this example shows that a small change in one parameter such as an 8% decrease in the translation velocity may translate into as much as an order-of-magnitude change in coating thickness uniformity. Finally, the effect of including a random phase shift, $\Delta\varphi = 10°$, increases the coating thickness variability from ± 0.3 μm to ± 1.0 μm.

A unique situation was discovered using this model. We termed this situation a "phase lock" condition, which satisfies Eq. 28. When it occurs, the coating path across the surface remains the same no matter how many times the nozzle passes back and forth across the surface. So, it produces a highly nonuniform coating thickness. In the third example, we intentionally set the translational speed v_z of 0.846 cm·s^{-1}, which had been calculated so as to satisfy Eq. 28, while keeping the other parameters the same as before. At this condition, the spray beam always passes over the same path no matter how many passes are made. The calculated results are shown in Figure 11. Figures 11a and 11b clearly show the highly nonuniform thickness. The surface is reminiscent of a moguled snowfield. The situation is somewhat similar to the case of the first example. The difference is, however, that in the first example case the nonuniformity is smoothed out after many passes, say $N \geq 40$, while in the "exact" phase lock case like this example, the nonuniformity never decreases no matter how many passes. Only random phase-shift conditions will smooth out the sharp peaks and valleys. Figure 11d indi-

cates such an effect already with a small $N = 10$ and a small random phase shift, $\Delta\varphi = 10°$; the coating thickness variability decreased from 5.3 μm to 3.1 μm.

Comparison with Experiment

Here we verify experimentally the model calculations described in the previous section as well as show that the phase-lock condition does exist. In these examples, the distance from the nozzle face to the cylinder surface, $L_1 = 2.22$ cm, the diameter of the tubular support, $2d = 2.54$ cm, the mass fraction of polymer concentration, $w = 0.3$, the polymer solution flow rate, $\dot{V} = 0.2$ cm$^3\cdot$min^{-1}, the rotational frequency, $f_R = 0.25$ s^{-1}, and the number of coating passes, $N = 16$, were set as constants. Only the translational speed was varied from $v_z = 0.6850$ s^{-1} to 0.7645 s^{-1}. Experimentally the spray-beam half-angle was determined to be essentially $\theta_0 = 0°$, and the effective spray-nozzle diameter was again $2r_0 = 0.556$ cm.

Based on model calculation, a translation velocity of 0.7645 cm$\cdot$s^{-1} was predicted to follow the same path across the support, phase-locked, leading to a nonuniform coating thickness. Further calculations showed that by reducing the translation velocity by only 10% to 0.6850 cm$\cdot$s^{-1}, a much more uniform coating thickness could be achieved. These two examples were chosen to validate the model.

The polymer thickness was calculated by measuring the color intensity with a digital scanner. The images were saved in bit format and the resulting tensor analyzed using Mathematica (Wolfram, 1999). The color intensity was normalized using the following relationship, $I = [0.299\ I_R + 0.587\ I_G + 0.114\ I_B]/255.0$, where I is the normalized color intensity (0 to 1.0) and I_R, I_G, and I_B are the red, green, and blue color intensities (1 to 255). To determine the calibration between polymer thickness and color intensity, several paper samples

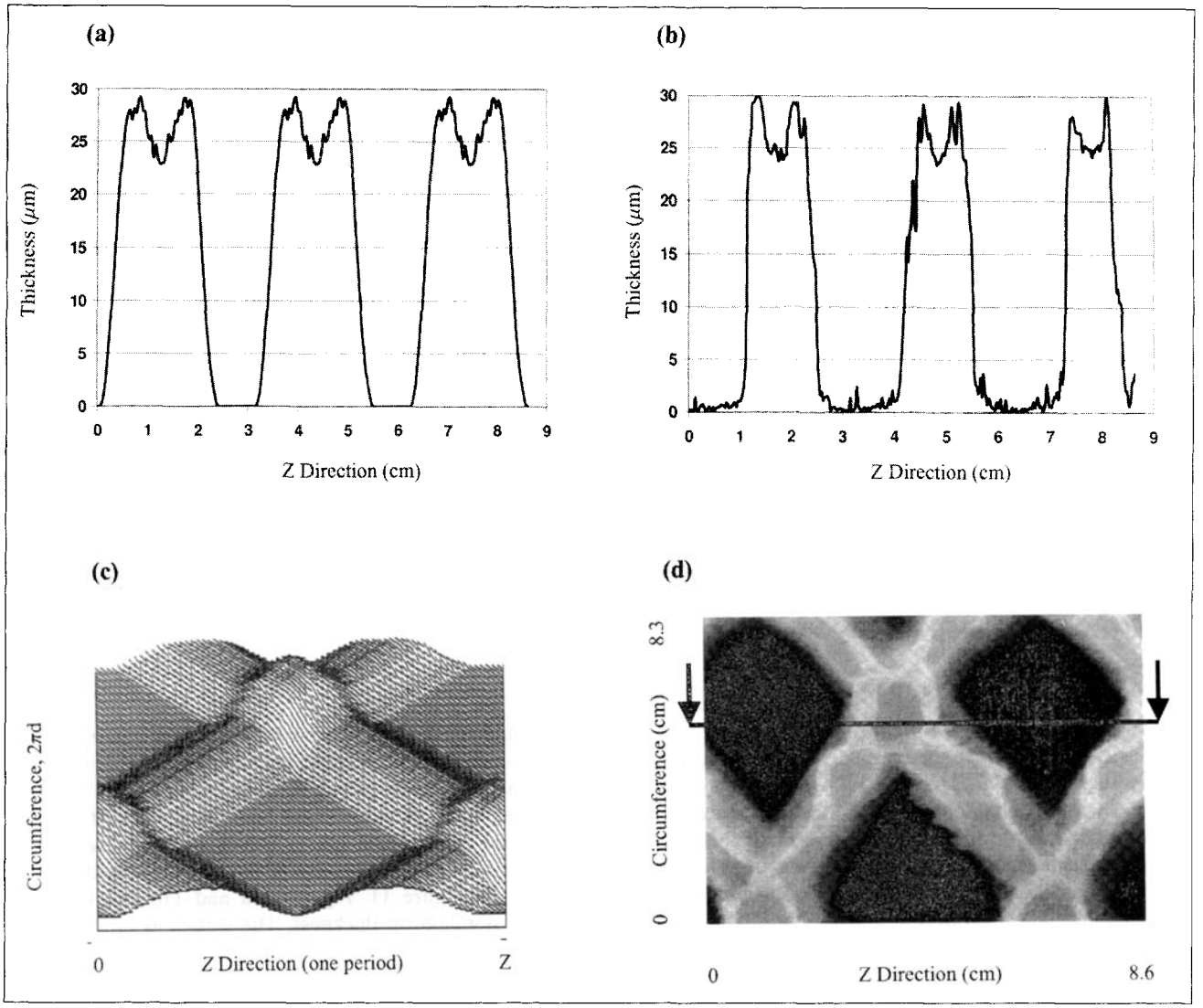

Figure 12. Results of computer simulation and experiment for $f_R = 0.25$ s^{-1}, $\dot{V} = 0.2$ cm$^3\cdot$min^{-1}; $N = 16$; $v_z = 0.7645$ cm$\cdot$s^{-1}.

(a) Axial view, calculation at $\varphi = 45°$; (b) axial view, experimental; (c) 3-D surface plot, calculation; (d) surface-image, experimental, cross section shown in (b) indicated by line.

were sprayed with a 30 mass percent poly(furfuryl) alcohol in acetone solution. The dried polymer mass per surface area ranged from 1 $mg \cdot cm^{-2}$ to 25.0 $mg \cdot cm^{-2}$. A polymer acetone solution density of 0.8880 $g \cdot cm^{-3}$ and a polymer density of 1.2114 $g \cdot cm^{-3}$ both at 25°C were used to calculate the polymer thickness, h. Each sample was scanned and a linear correlation of polymer thickness and color intensity was determined: $h(\mu m) = 44.451I - 2.304$ for $(0 < I < 0.7)$.

Figures 12a and 12b compare the calculated and experimental thickness profiles in the z-direction at $v_z = 0.7645$ cm $\cdot s^{-1}$. The model accurately predicts the nonuniform coating thickness shown by experiment with an average thickness of 26 μm in the coated areas and no coverage, thickness of 0 μm in the uncoated areas. The small difference in the width of the peaks is due to the slight difference in phase-angle cut. Figures 12c and 12d compare the calculated and experimental surface images where the phase-locked condition can easily be seen, even after sixteen coating passes. The model reproduces both the qualitative and quantitative features of the surface.

Figures 13a and 13b compare the axial thickness calculations with experiment for the case when $v_z = 0.6850$ cm $\cdot s^{-1}$. Again the model clearly predicts the more uniform coating with an average thickness of 17.5 ± 2.5 μm. The calculated and experimental surface images shown in Figures 13c and 13d also confirm the improved uniformity in the coating thickness.

Discussion

We have demonstrated the usefulness of these model calculations for predicting the film-thickness morphology, and we have shown and experimentally verified two different examples with the operating parameter v_z as a single variable.

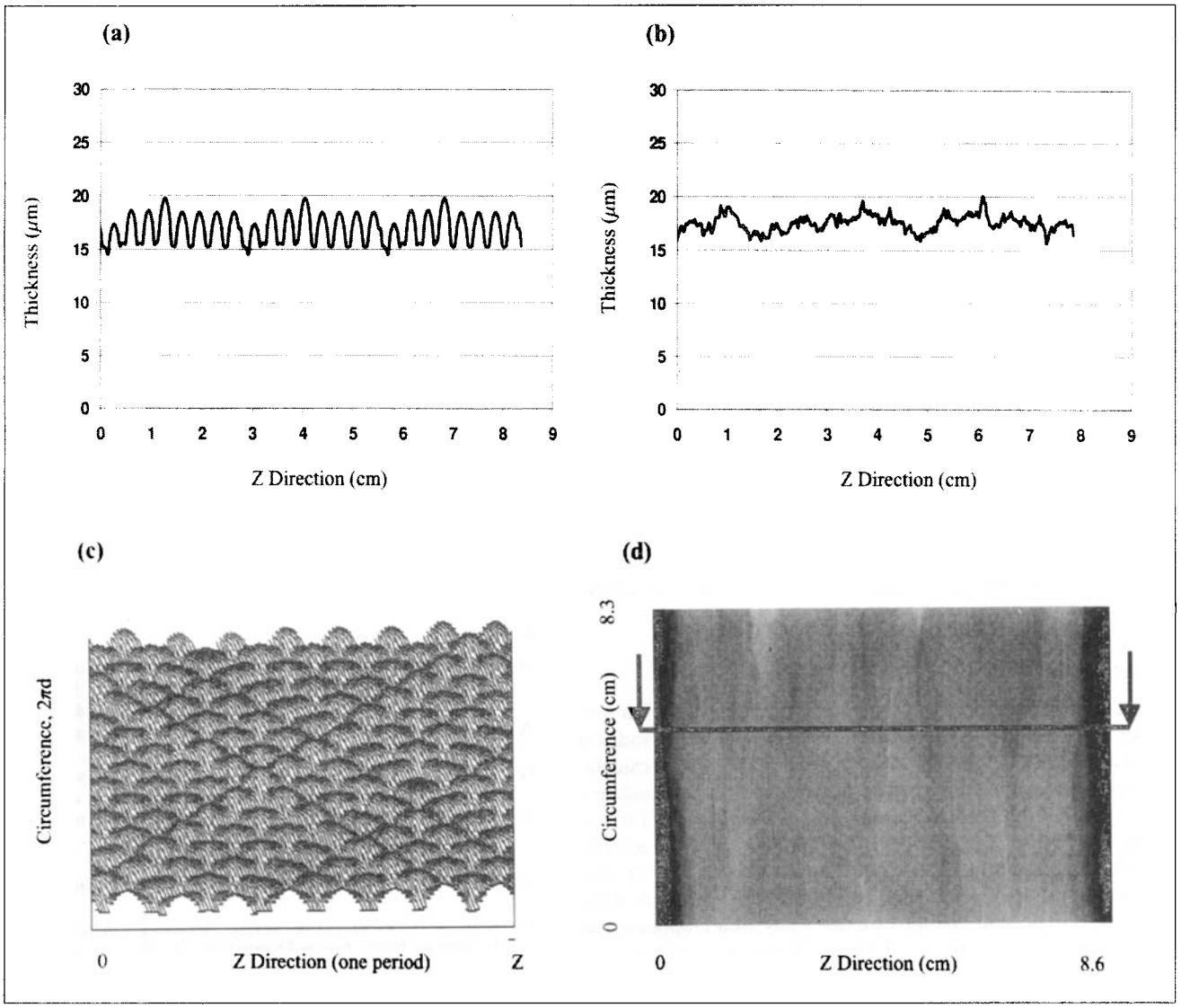

Figure 13. Results of computer simulation and experiment with the same parameters as those in Figure 12, except $v_z = 0.6850$ cm $\cdot s^{-1}$.

(a) Axial view, calculation at $\varphi = 45°$; (b) axial view, experimental; (c) 3-D surface plot, calculation; (d) surface-image, experimental, cross section shown in (b) indicated by line.

Similar calculations with other operating parameters as variables can easily be made and be used for finding the optimal experimental conditions in multiparameter controls. The value of the model is clear, when we observe the high sensitivity of the thickness and uniformity of the coated films to the operating parameters. Small variations in experimental conditions may lead to large changes in film morphology, such as the highly nonuniform film thickness by a phase-lock (frozen) condition.

The phase-lock condition occurs for multiple coating passes whenever the values of the operating parameters satisfy or nearly satisfy this condition

$$\frac{\Delta\varphi_0}{2\pi} = \frac{\omega\,|\,z_0\,|}{\pi v_z} = \frac{2f_R\,|\,z_0\,|}{v_z} = \frac{n}{m}, \quad n, m = \text{integer},$$

where z_0 is equal to either R (in the case of $\theta_0 = 0$) or R_x ($\theta_0 > 0$). This equation is, however, quite complicated because of the presence of z_0. In the case of $\theta_0 = 0$, z_0 becomes $R = r_0$ (Figures 2 and 3), while in the case of $\theta_0 > 0$, $z_0 = R_x$ is a root of Eq. 25 with Eq. 23 and becomes a function of d, L_1, r_0, and θ_0. Then values of r_0 and θ_0 depend in turn on the flow rate $\dot{V}$ and the concentration w of the polymer solution, as discussed previously in the model-development section. So, the phase-lock condition is a rather complicated function of all the experimental operating parameters: d, L_1, $\dot{V}$, w, f_R, and v_z in N multiple passes. The phase-lock coating is undesirable for our present purpose. Fortunately, however, it is only serious if the pathway across the tubular surface is repeated after only a few passes (that is, when the integer values of n and m are relatively small numbers), resulting in large variations in the coating-thickness uniformity.

Finally, although it is obvious, it may be worthwhile mentioning that the present model formulation is equally applicable for the case of a rotating cylinder with no translation, but having instead a translating nozzle head. Also, the model can be used for any spray nozzle and polymer solution, as long as the characteristics of the spray beam are experimentally obtained, as described in the experimental section. Additional work on the impact the polymer coating uniformity has on carbon membrane performance will be described in the future.

Summary

A general mathematical model has been developed to predict the film thickness of polymers coated on a cylindrical substrate with an ultrasonic spray nozzle. The model calculations reveal various unexpected features of the film-thickness morphology. The model appears to be a useful tool for setting the proper experimental parameters for the desired thickness and uniformity of the film of interest, and it provides us with important insights on the coating process. Also, use of the present model extends many other applications where the precise control of film thickness is required for a cylindrical substrate in various polymer-coating systems.

Acknowledgments

Funding for this research was provided by the DuPont Company, the State of Delaware Research Partnership, and the Department of Energy, Office of Basic Energy Sciences. Special thanks go to Dr. Mark E. Lewittes and Mr. Joseph Nestlerode, Central Research and Development, DuPont Experimental Station, for their assistance with scanning and illustrations.

Notation

$\bar{c}$ = average speed of spray particles
d = radius of cylinder
f_R = cylinder rotation per unit time (rotational frequency)
h = thickness of polymer film
L = distance from point source to cylinder center line
L_0 = distance from point source to nozzle face
L_1 = distance from nozzle face to cylinder surface
L' = distance of coverage measured in the axial direction
l = distance from point source to arbitrary point of cylinder surface
$\bar{m}$ = average mass of spray particles
N = number of coating passes across cylindrical support, or number of particles
r_0 = effective spray radius at nozzle face
R = spray shadow length
R_x = spray shadow length
t = time variable
V = volume
$\dot{V}$ = volumetric flow rate of polymer solution
v_z = translational velocity of cylinder
w = mass fraction of polymer in polymer solution
x = Cartesian coordinate—x-direction
y = Cartesian coordinate—y-direction
z = Cartesian coordinate—z-direction
z_0 = maximum integration range: equal to $R(\theta_0 = 0)$ or $R_x(\theta_0 > 0)$
z_i = crossing point of spray-beam boundary in the z-coordinate

Greek Letters

α_i = initial or final phase angle of integration for each coating pass
β = angle variable in the xz-plane
φ = phase angle of cylinder rotation, or angle variable in the yz plane
γ = angle between spray-beam direction and radial direction of cylinder
θ = angle of spray beam at arbitrary direction
θ_0 = angle of spray-beam spread
θ_d, θ_x = limiting angle of spray beam
ρ = polymer density
ρ_0 = polymer solution density
ρ_s = solvent density
ω = angle velocity (angular frequency) $\omega = 2\pi f_R$

Literature Cited

Acharya, M., B. A. Raich, H. C. Foley, M. P. Harold, and J. J. Lerou, "Metal Supported Carbogenic Molecular Sieve Membranes—Synthesis and Applications," *Ind. Eng. Chem. Res.*, **8**, 2924 (1997).

Acharya, M., and H. C. Foley, "Spray Coating of Nanoporous Carbon Membranes for Air Separation," *J. Memb. Sci.*, **161**, 1 (1999).

Acharya, M., and H. C. Foley, "Transport in Nanoporous Carbon Membranes: Experiments and Analysis," *AIChE J.*, **46**, 5 (2000).

Chen, Y. D., and R. T. Yang, "Preparation of Carbon Molecular Sieve Membrane and Diffusion of Binary Mixtures in the Membrane," *Ind. Eng. Chem. Res.*, **93**, 3146 (1994).

Ensminger, D., *Ultrasonics; The Low-and High-Intensity Applications*, Marcel Dekker, Inc., New York (1973).

Fasching, M., F. Prinz, and L. Weiss, "Planning Robotic Trajectories for Thermal Spray Shape Deposition," *J. Thermal Spray Technol.*, **2**, 45 (1993).

Figueroa, H., and O. Diaz, "Thermal Spray Modeling of Flat Surfaces and Cylinders," *Thermal Spray Coating Proc. Nat'l. Spray Conf.*, 4th, T. F. Bernecki, ed., ASM, Materials Park, OH, 549 (1992).

Frederick, J. R., *Ultrasonic Engineering*, Wiley, New York (1965).

Goedjen, J., R. Miller, W. Brindley, and G. Leissler, "A Simulation Technique for Predicting Thickness of Thermal Sprayed Coatings,"

NASA Tech. Rep. ARL-TR-762, Lewis Research Center, Cleveland, OH (1995).
Hansbo, A., and P. Nylen, "Models for the Simulation of Spray Deposition and Robot Motion Optimization in Thermal Spraying of Rotating Objects," *Surface Coat. Technol.*, **122**, 191 (1999).
Hueter, T. F., and R. H. Bolt, *Sonics*, Wiley, New York (1960).
Hutchinson, J. W., and Z. Suo, "Mixed Mode Cracking in Layered Materials," *Adv. Appl. Mech.*, **29**, 63 (1991).
Kasakabe, K., M. Yamamoto, and S. Morooka, "Gas Permeation and Micropore Structure of Carbon Molecular Sieving Membranes Modified by Oxidation," *J. Memb. Sci.*, **149**, 59 (1998).
Leigh, S., and C. Berndt, "Evalutation of Off-Angle Thermal Spray," *Surface Coat. Technol.*, **89**, 213 (1997).
Montillet, D., E. Dombere, and P. Valentin, "Deposit Model for Off-line Programming in a Spray Process," *Thermal Spray: Meeting the Challenges of the 21st Century*, C. Coddett, ed., ASM International, Materials Park, OH, p. 905 (1998).
Nylen, P., I. Fransson, A. Wretland, and N. Martensson, "Coating Thickness Prediction and Robot Trajectory Generation of Thermal Sprayed Coatings," *Thermal Spray: Practical Solutions for Engineering Problems*, C. C. Bertndt, ed., ASM International, Materials Park, OH, p. 693 (1996).
Persoons, W., and H. Van Brussel, "CAD-Based Robotic Coatings of Highly Curved Surfaces," Preprint, Dept. of Mechanical Engineering, Division PMA, Katholieke Universiteit Leuven, Heverlee, Belgium (1993).
Rao, M. B., and S. Sircar, "Nanoporous Carbon Membranes for Separation of Gas Mixtures by Surface Selective Flow," *J. Memb. Sci.*, **85**, 253 (1993).
Rao, M. B., and S. Sircar, "Performance and Pore Characterization of Nanoporous Carbon Membranes for Gas Separation," *J. Memb. Sci.*, **110**, 109 (1996).
Shiflett, M. B., and H. C. Foley, "Ultrasonic Deposition of High-Selectivity Nanoporous Carbon Membranes," *Science*, **285**, 1902 (1999).
Shiflett, M. B., J. F. Pedrick, S. R. McLean, S. Subramoney, and H. C. Foley, "Characterization of Supported Nanoporous Carbon Membranes," *Adv. Mater.*, **12**, 21 (2000).
Shiflett, M. B., and H. C. Foley, "Reproducible Production of Nanoporous Carbon Membranes," *Carbon*, **39**(9), 1421 (2001).
Shiflett, M. B., and H. C. Foley, "On the Preparation of Supported Nanoporous Carbon Membranes," *J. Memb. Sci.*, **179**, 275 (2000).
Singh-Ghosal, A., and W. J. Koros, "Air Separation Properties of Flat Sheet Homogenous Pyrolytic Carbon Membranes," *J. Memb. Sci.*, **174**, 177 (2000).
Suslick, K. S., *Ultrasound—Its Chemical, Physical, Biological Effects*, VCH, New York (1988).
Vivekanandhan, T., A. Kashani, and R. Echempati, "Computer-Aided Torch Trajectory Generation for Automated Coating of Parts with Complex Surfaces," *J. Thermal Spray Technol.*, **3**, 208 (1994).
Wolfram, S., *The Mathematica Book*, 4th ed., Wolfram Media/Cambridge Univ. Press, Cambridge (1999).

Manuscript received July 27, 2000, and revision received Mar. 6, 2001.